ELSEVIER

Alzheimer's & Dementia: Diagnosis, Assessment & Disease Monitoring 10 (2018) 221-231

Alzheimer's & Dementia

Special Section: State of the Field: Advances in Neuroimaging from the 2017 Alzheimer's Imaging Consortium

Topographic staging of tau positron emission tomography images

Adam J. Schwarz[a,b,c,*], Sergey Shcherbinin[a], Lawrence J. Slieker[a], Shannon L. Risacher[b,d], Arnaud Charil[a], Michael C. Irizarry[a], Adam S. Fleisher[a], Sudeepti Southekal[e], Abhinay D. Joshi[e], Michael D. Devous, Sr.[e], Bradley B. Miller[a], Andrew J. Saykin[b,d], For the Alzheimer's Disease Neuroimaging Initiative[1]

[a]*Eli Lilly and Company, Indianapolis, IN, USA*
[b]*Department of Radiology and Imaging Sciences, Indiana University School of Medicine, Indianapolis, IN, USA*
[c]*Department of Psychological and Brain Sciences, Indiana University, Bloomington, IN, USA*
[d]*Indiana Alzheimer Disease Center, Indiana University School of Medicine, Indianapolis, IN, USA*
[e]*Avid Radiopharmaceuticals (a Wholly Owned Subsidiary of Eli Lilly and Company), Philadelphia, PA, USA*

Abstract

Introduction: It has been proposed that the signal distribution on tau positron emission tomography (PET) images could be used to define pathologic stages similar to those seen in neuropathology.
Methods: Three topographic staging schemes for tau PET, two sampling the temporal and occipital subregions only and one sampling cortical gray matter across the major brain lobes, were evaluated on flortaucipir F 18 PET images in a test-retest scenario and from Alzheimer's Disease Neuroimaging Initiative 2.
Results: All three schemes estimated stages that were significantly associated with amyloid status and when dichotomized to tau positive or negative were 90% to 94% concordant in the populations identified. However, the schemes with fewer regions and simpler decision rules yielded more robust performance in terms of fewer unclassified scans and increased test-retest reproducibility of assigned stage.
Discussion: Tau PET staging schemes could be useful tools to concisely index the regional involvement of tau pathology in living subjects. Simpler schemes may be more robust.

Keywords: Tau; PET; Flortaucipir; Alzheimer; Staging; Stage; Classification; Image; Braak; AV-1451; T807

1. Introduction

Alzheimer's disease (AD) is defined neuropathologically by the presence of amyloid β plaques and neurofibrillary tangles (NFTs) of misfolded phosphorylated tau protein [1–3]. Whereas amyloid plaques are widespread in the neocortex [2], in sporadic AD, NFTs present in characteristic patterns that suggest tau pathology begins in the entorhinal cortex and then spreads in a largely stereotypical fashion first into the inferior and lateral temporal cortices, followed by regions in the parietal and frontal lobes, and finally the primary sensory cortices in end-stage disease [1]. This has been codified topographically in neuropathologic tau staging schemes [4,5].

The recent development of radiolabeled positron emission tomography (PET) ligands for tau tangles [6–8] has enabled NFTs to be imaged in the brains of living humans. Initial studies have demonstrated that in vivo tau PET

[1]Data used in preparation of this article were obtained from the Alzheimer's Disease Neuroimaging Initiative (ADNI) database (adni.loni.usc.edu). As such, the investigators within the ADNI contributed to the design and implementation of ADNI and/or provided data but did not participate in analysis or writing of this report. A complete listing of ADNI investigators can be found at: http://adni.loni.usc.edu/wp-content/uploads/how_to_apply/ADNI_Acknowledgement_List.pdf.

*Corresponding author. Tel.: 317-405-7494.
E-mail address: a.schwarz@lilly.com

https://doi.org/10.1016/j.dadm.2018.01.006

images show diverse patterns of tracer binding consistent with those observed in neuropathologic studies, providing strong prima facie evidence that these ligands reflect the distribution of tau pathology in the living brain [9–13].

The availability of these PET tracers and other biomarkers has stimulated the formulation of classification frameworks for clinical AD research based on sequential biological changes in the brain [14–20]. These criteria enable the severity of cognitive and functional impairment to be complemented by objective measures of disease pathology and are refining the concepts of both diagnosis and stage in the study of AD. To date, much of the emphasis has been on dichotomized biomarker measurements, indicating the presence or absence of different pathological changes [21], exemplified most recently by the A/T/N system based on abnormal amyloid, tau, and/or neurodegeneration [16]. However, the stereotypical patterns of NFT localization also allow for a more granular regional staging of tau pathology per se, and neuropathologic observations can inform image-based classification or staging schemes that can be applied to tau PET images in vivo [10,11]. These topographic image classification schemes provide a concise summary of the anatomical distribution of tracer binding that conveys the extent of regional involvement. Interpretation of these profiles within a staging framework rests on the assumption that certain profiles succeed others as the disease progresses. Findings in both neuropathology studies and emerging data with tau PET tracers support this view, with the degree of regional involvement associated with amyloid status, cognitive performance, and clinical disease stage [10,13,22,23].

One of these recently described staging algorithms [10] is based on small regions of interest (ROIs) in the anterior temporal and occipital lobes and classification rules that match as accurately as possible the 6-stage operationalized neuropathologic staging scheme proposed by Braak *et al.* [4]. This approach confirmed the predominance of stereotypical tau PET patterns in individuals across the AD spectrum, but 7% of the scans in that study were not able to be matched to one of the a priori–defined patterns, which could be a limitation for prospective use of that method in clinical research. Moreover, the very small ROIs in that scheme are potentially sensitive to variations in image preprocessing, atrophy, and experimental noise. In addition, the medial temporal lobe (MTL) regions distinguishing stages 1–3 are potentially prone to contamination from adjacent extraparenchymal signals (e.g., optic nerve) and to tracer binding in the choroid plexus. As a result, it may be difficult to reliably distinguish between stages 1, 2, and 3 using that method. Finally, the more advanced stages 5–6 do not capture the variability across subjects in the broader neocortical involvement of tau in the later stages of AD.

Motivated by these limitations, we propose two simpler tau PET staging schemes that use fewer, larger ROIs and simplified decision rules. The first of these also targets regions restricted to the anterior temporal and occipital lobes but uses larger atlas-based masks and consolidates regions in the MTL. The second is based on the average signal in each of the temporal, parietal, and frontal lobes, thus sampling more of the cortex overall. The rationale for these alternative schemes is to improve robustness to image noise (e.g., test-retest), simplify implementation, and minimize unclassifiable scans. In the case of the second scheme, the rationale was also to provide more dynamic range in the assigned stages for cases with more widespread tau load. Here, we evaluate these two schemes, in comparison to that previously described [10], applied to flortaucipir F 18 scans acquired in a test-retest scenario and in the Alzheimer's Disease Neuroimaging Initiative 2 (ADNI-2) study. In addition to profiling each scheme as a staging tool, we also assess the three staging schemes when dichotomized to define each scan as tau positive or tau negative.

2. Methods

2.1. Data sets

Data from four tau imaging studies were used to form three data sets for the present analysis. The first data set was a set of flortaucipir F 18 scans from N = 14 young healthy individuals visually and quantitatively (bilateral entorhinal cortex standardized uptake value ratio [SUVr] < 1.2) determined to be tau negative and used as a reference sample [10]. These scans were drawn from an exploratory phase 1 study and from a larger phase 2 study (NCT02016560) undertaken as part of Avid Radiopharmaceuticals' clinical development program for the flortaucipir F 18 PET radiotracer. The second data set was a test-retest study (N = 21, retest interval 4–28 days) in participants assessed as cognitively normal (CN) or diagnosed with either mild cognitive impairment (MCI) or symptomatic AD [24]. This data set was used to assess within-subject reproducibility of the staging algorithms. The third data set comprised N = 98 participants in the ADNI-2 that received a flortaucipir F 18 PET scan. Further details of the ADNI consortium are provided in the Supplementary Material. Amyloid positivity (A+) in ADNI-2 was determined from a Florbetapir F 18 PET scan, processed by the ADNI PET core (University of California, Berkeley) and with a cortical SUVr > 1.11. All subjects gave informed consent.

2.2. PET image acquisition and processing

Participants received an intravenous injection of approximately 10 mCi flortaucipir F 18, and PET images from four 5-minute frames between 80 and 100 minutes following the radiotracer injection were analyzed.

The four 5-minute flortaucipir F 18 PET scans were corrected for motion, averaged, and coregistered to the individual participant's accompanying T1-weighted magnetic resonance imaging (MRI) scan. For the ADNI-2 study, preprocessed flortaucipir F 18 PET scans were downloaded from the ADNI Laboratory of Neuro Imaging (http://adni.loni.usc.edu) site. The MRI scan was spatially normalized to the MNI152 T1 MRI template, and this transformation

was then applied to the same participant's tau PET scan. All tau PET images were then transformed into SUVr images using a cerebellar gray matter reference region.

2.3. Tau classification algorithms

Each of the classification schemes was based on binarizing the mean SUVr signals within a predefined set of ROIs and then seeking to match the resulting profile with expected patterns. The three tau PET staging schemes evaluated were as follows:

- Temporal-Occipital Classification (TOC): This recently published approach [10] was explicitly designed to mimic as closely as possible, in terms of brain regions sampled and decision rules, the Braak 2006 operationalized neuropathologic guidelines [4]. This scheme uses small ROIs localized around the anterior temporal lobe (hippocampus, transentorhinal cortex, fusiform cortex, middle temporal gyrus, and superior temporal gyrus) and in the occipital lobe (extrastriate and primary [striate] visual cortex).
- Simplified Temporal-Occipital Classification (STOC): This approach was developed as a simplified version of TOC, modified to use fewer and larger ROIs from standard atlases, located in the medial, lateral, and superior temporal lobes and in the primary visual cortex, as well as simpler decision rules.
- Lobar classification (LC): This approach is simpler than both TOC and STOC and uses whole-lobar average signals from the temporal (T), parietal (P), and frontal (F) lobes. This scheme has the fewest and largest ROIs, sampling most of the cortical gray matter and even simpler decision rules to assign stages.

For the TOC scheme only, the tau PET images were gray matter masked for compatibility with the published method [10]. This was achieved by thresholding each individual participant's gray matter tissue probability map at 25% and binarizing to yield an individualized gray matter mask. Gray matter masking was not applied to the regions used in the STOC and LC schemes as preliminary analyses suggested that this did not improve performance. The ROIs are illustrated in Fig. 1 and are further described in the Supplementary Material.

For each scheme, both stereotypical and atypical expected profiles (binary patterns across the staging ROIs) were predefined (Tables 1–3). In the case of both TOC and STOC, these profiles included hippocampal-sparing or medial temporal–sparing variants of the more advanced stage patterns. In the case of LC, the number of permutations was sufficiently low that we enumerated all possible profiles, with those expected to reflect the stereotypical progression of AD being T−P−F− → T+P−F− → T+P+F− → T+P+F+. Atypical patterns included T− with P+ or F+, and T+P−F+. For each scheme, the profiles for each hemisphere were matched independently to the predefined set of permitted patterns, and the most advanced profile was assigned to the scan.

2.4. Thresholds for binarization

Thresholds for all schemes were determined on an ROI-specific basis [25] with respect to the mean and standard deviation flortaucipir F 18 SUVr values from 14 younger healthy control subjects (age 21–31 years, average 26.2 years) determined to be "tau negative" based on visual inspection (the same set used in ref. [10]). Thresholds were determined for each scheme so as to yield comparable absolute SUVr

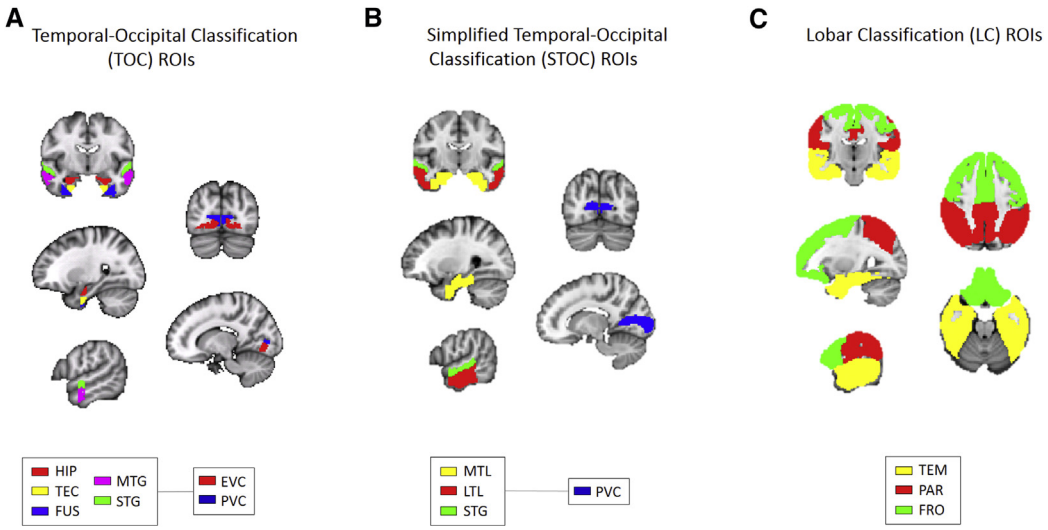

Fig. 1. Visualization of the regions of interest (ROIs) used in the three staging schemes. (A) ROIs used in TOC, (B) ROIs used in STOC, and (C) ROIs used in LC. Abbreviations: HIP, hippocampus; TEC, transentorhinal cortex; FUS, fusiform gyrus; MTG, middle temporal gyrus; STG, superior temporal gyrus; EVC, extrastriate visual cortex; PVC, primary visual cortex; MTL, mesial temporal lobe; LTL, lateral temporal lobe; TEM, temporal lobe; PAR, parietal lobe; FRO, frontal lobe; TOC, Temporal-Occipital Classification; STOC, Simplified Temporal-Occipital Classification; LC, lobar classification.

Table 1
Predefined patterns for the TOC scheme*

Stage	Hippocampus (HIP)	Transentorhinal cortex (TEC)	Fusiform gyrus (FUS)	Middle temporal gyrus (MTG)	Superior temporal gyrus (STG)	Extrastriate visual cortex (EVC)	Primary visual cortex (PVC)
0	**−**	**−**	**−**	**−**	**−**	**−**	**−**
1	**−**	**+**	**−**	**−**	**−**	**−**	**−**
2	**+**	**+**	**−**	**−**	**−**	**−**	**−**
3	**+**	**+**	**+**	**−**	**−**	**−**	**−**
3 (HIP sparing)	−	+	+	−	−	−	−
4	**+**	**+**	**+**	**+**	**−**	**+**	**−**
4 (HIP sparing)	−	+	+	+	−	+	−
4 (EVC sparing)	+	+	+	+	−	−	−
4 (HIP and EVC sparing)	−	+	+	+	−	−	−
5	**+**	**+**	**+**	**+**	**+**	**+**	**−**
5 (HIP sparing)	−	+	+	+	+	+	−
5 (EVC sparing)	+	+	+	+	+	−	−
5 (HIP and EVC sparing)	−	+	+	+	+	−	−
6	**+**	**+**	**+**	**+**	**+**	**+**	**+**
6 (HIP sparing)	−	+	+	+	+	+	+

Abbreviations: TOC, Temporal-Occipital Classification; ROI, region of interest.
NOTE. Typical profiles are shown in bold and permitted atypical profiles in italics.
From ref. [10].
*A '+' symbol indicates that the average signal in that ROI is above threshold, whereas a '−' symbol indicates that it is below threshold.

thresholds as previously published for TOC. For TOC, the threshold in each ROI was defined as 2.5 standard deviations above the mean of this reference set; this resulted in threshold SUVr values ranging from 1.22 to 1.36 (average 1.28) [10]. For STOC, to obtain threshold SUVr values with an average of 1.28 (range 1.24 to 1.31) as obtained for the TOC approach, a criterion of three standard deviations above the mean of the reference set was used. For the LC staging approach, threshold SUVr values with a similar average of 1.28 (range 1.26 to 1.30) were also obtained using a criterion of three standard deviations above the mean of the reference set. The threshold values, and a comparison with results obtained with threshold values calculated as 2.5 standard deviations above the mean for all three schemes, are provided in the Supplementary Material.

For the purposes of dichotomizing scans to "tau negative" (T−) or "tau positive" (T+) based on regional involvement, we defined tau negative as stage 0–3 in TOC, stage 0–1 in STOC, and stage 0 in LC and accordingly, tau positive as stage 4–6 in TOC, stage 2–4 in STOC, and stage 1–3 in the LC scheme (irrespective of whether the profiles were typical or atypical).

2.5. Statistical analysis

Test-retest reliability was assessed by the percent of participants whose stage assignment was identical on both test and retest scans. The robustness of the staging schemes was assessed by the number of scans that were able to be matched to one of the predefined binarized ROI profiles. Stereotypy of each ROI profile was quantified in the ADNI data set by calculating the Spearman rank correlation between the predicted rank order of SUVr values and the measured rank order of the difference between the individual region SUVr values and their corresponding region-specific thresholds. The predicted rank order was the same as the typical order of regional involvement inscribed in the staging rules (Tables 1–3). The average Spearman correlation across

Table 2
Predefined patterns and staging rules for the STOC scheme*

Stage	Medial temporal lobe (MTL)	Lateral temporal lobe (LTL)	Superior temporal gyrus (STG)	Primary visual cortex (PVC)
0	**−**	**−**	**−**	**−**
1	**+**	**−**	**−**	**−**
2	**+**	**+**	**−**	**−**
2 (MTL sparing)	−	+	−	−
3	**+**	**+**	**+**	**−**
3 (MTL sparing)	−	+	+	−
4	**+**	**+**	**+**	**+**
4 (MTL sparing)	−	+	+	+

Abbreviations: STOC, Simplified Temporal-Occipital Classification; ROI, region of interest.
NOTE. Typical profiles are shown in bold and permitted atypical profiles in italics.
*A '+' symbol indicates that the average signal in that ROI is above threshold, whereas a '−' symbol indicates that it is below threshold.

Table 3
Predefined profiles and staging rules for the LC scheme*

Stage	Temporal lobe (TEM)	Parietal lobe (PAR)	Frontal lobe (FRO)
0 (T−P−F−)	**−**	**−**	**−**
1 (T+P−F−)	**+**	**−**	**−**
2 (T+P+F−)	**+**	**+**	**−**
2 (T−P+F−)	−	+	−
3 (T+P+F+)	**+**	**+**	**+**
3 (T+P−F+)	+	−	+
3 (T−P−F+)	−	−	+
3 (T−P+F+)	−	+	+

Abbreviations: LC, lobar classification; ROI, region of interest; T, temporal; P, Parietal; F, Frontal.

NOTE. Typical profiles are shown in bold and permitted atypical profiles in italics.

*A '+' symbol indicates that the average signal in that ROI is above threshold, whereas a '−' symbol indicates that it is below threshold.

scans is reported for each scheme. Additional statistical analyses on the ADNI data set were conducted in JMP v12.1 (SAS, Cary, NC, USA). The relationship between assigned stages and amyloid status was assessed using an ordinal logistic regression model for each staging scheme, with age, disease category, and sex as additional covariates. The relationships between regional SUVr and global cortical SUVr values, and between assigned stages and global cortical SUVr values, were assessed using Pearson pairwise correlations. An alpha level of 0.05 (two sided) was used as a threshold for statistical significance.

3. Results

3.1. Participant characteristics

Both the test-retest and ADNI-2 data sets contained participants ranging from CN to demented. The test-retest data set comprised N = 5 (CN, age [mean ± SD] 64.8 ± 9.2 years), 6 MCI (age 70.3 ± 5.9 years), and 10 AD (age 74.4 ± 7.3 years) participants. The ADNI-2 sample comprised N = 34 CN (age 74.6 ± 7.4 years; 14 amyloid positive [A+], 19 amyloid negative [A−]), 12 subjective memory complaints (age 71.7 ± 4.6 years; 5 A+, 7 A−), 24 early MCI (age 75.0 ± 7.5 years; 15 A+, 9 A−), 18 late MCI (age 76.9 ± 8.6 years; 9 A+, 7 A−), and 10 AD (age 78.4 ± 5.8 years; 9 A+, 1 A−) participants. In the ADNI-2 data set, the amyloid status was unknown for 4% (4/98) of participants. The characteristics of the participants are further tabulated in the Supplementary Material.

3.2. Reliability and consistency of staging schemes (test-retest data set)

When applied to the test-retest data set, the TOC scheme matched 86% (18/21) of both the test and retest scans to a predefined pattern, with 10% (2/21) of each set being an atypical profile. Across the test and retest scans, the TOC scheme assigned the same stage to 81% (17/21) of the subjects (Table 4). Of the other four, one moved from unclassified to stage 4, one from stage 4 (hippocampal sparing) to unclassified, one from stage 0 to 4 (hippocampus and extrastriate visual cortex sparing), and one from stage 6 to 4.

The STOC scheme matched 100% (21/21) of the scans to a predefined pattern in both test and retest sessions, with 5% (1/21) of each set being atypical profiles. It assigned the same pattern to 86% (18/21) of the subjects across the test and retest scans (Table 4). Of the other three, one moved from stage 3 to 4, one from stage 1 to 0, and one from stage 0 to 2.

The LC scheme matched 100% (21/21) of the scans in both test and retest sessions to a predefined stereotypical pattern and assigned the same pattern to 95% (20/21) of the subjects across test and retest scans (Table 4). The participant whose assigned stage changed moved from stage 1 to 0.

The participants whose stage changed under the TOC and STOC schemes were different individuals. The participant whose stage changed from 1 to 0 under the LC scheme was the same participant whose stage changed from 1 to 0 under the STOC scheme.

3.3. Anatomical profiles (ADNI-2 data set)

In the ADNI sample, the TOC scheme matched 79% (77/98) of the scans to a predefined stage pattern, with 11% (11/98) being atypical variant profiles (Table 4). In contrast, both the STOC and LC topographical staging schemes matched

Table 4
Test-retest stability and completeness of matching to predefined profiles for the three staging schemes

Data set and metric	TOC	STOC	LC
Test-retest, N (%) of subjects with unchanged stage	17/21 (81%)	18/21 (86%)	20/21 (95%)
Test-retest scan 1, N (%) matching predefined profiles including permitted variants	18/21 (86%) [incl. 2/21 (10%) atypical]	21/21 (100%) [incl. 1/21 (5%) atypical]	21/21 (100%)
Test-retest scan 2, N (%) matching predefined profiles including permitted variants	18/21 (86%) [incl. 2/21 (10%) atypical]	21/21 (100%) [incl. 1/21 (5%) atypical]	21/21 (100%)
ADNI-2, N (%) matching predefined profiles including permitted variants	77/98 (79%) [incl. 11/98 (11%) atypical]	98/98 (100%) [incl. 5/98 (5%) atypical]	98/98 (100%)

Abbreviations: TOC, Temporal-Occipital Classification; STOC, Simplified Temporal-Occipital Classification; LC, lobar classification; ADNI-2, Alzheimer's Disease Neuroimaging Initiative 2.

tau PET scans to a predefined profile for 100% (98/98) of participants, although for STOC, 5% (5/98) of these were MTL-sparing variants (Table 4).

The ROI profiles associated with each stage are illustrated in Fig. 2. For the TOC scheme, the atypical variants of the stage 3 profiles were primarily hippocampal sparing, whereas the atypical variants of the stage 4 and 5 profiles were mainly characterized by sparing of the extrastriate visual cortex (Fig. 2B). For the STOC scheme, in contrast to their stereotypical stage counterparts, the MTL-sparing profiles were overall perithreshold (Fig. 2C). With the LC scheme, using temporal, parietal, and frontal lobes only, 100% (98/98) of the cases evidenced a stereotypical profile (Table 4).

Mean SUVr images for all subjects assigned the same stage are shown in Fig. 3, illustrating the whole brain patterns beyond the specific ROIs used for classification. The precuneus and posterior cingulate cortex, along with the orbitofrontal and anterior cingulate cortices, are minimally involved for stages classified as having tau in the MTL but not the lateral temporal lobe, but have notably increased signal at stages corresponding to the presence of tau outside the MTL (TOC stage $\geq$4 and STOC stage $\geq$2).

The degree of stereotypy in the sequential regional involvement of the regions used in each of the staging schemes is illustrated in Fig. 4. In all three schemes, higher global cortical SUVr (which ranged from 0.89 to 1.78) was associated with positivity in more of the staging regions, with more of the "later" regions being positive as the global SUVr increases. SUVr values in the individual ROIs were also associated with global cortical SUVr (R^2 = 0.15–0.76 for TOC, 0.28–0.81 for STOC, and 0.76–0.87 for LC), with the weakest associations in TOC and STOC observed for the occipital cortex ROIs. When the scans were ranked by the order in which each region becomes positive, in the order encoded in the staging schemes, the patterns reveal a predominant stereotypy overall, wherein "later" regions turn positive only when "earlier" regions are already so. This relationship was cleanest for the LC scheme. Consistent with these observations, when quantified using Spearman rank correlations, the average stereotypy values in the left and right hemispheres were 0.32 and 0.36 for TOC, 0.76 and 0.74 for STOC, and 0.89 and 0.91 for the LC scheme.

The assigned stages were significantly associated with global cortical SUVr for all three schemes (TOC: R^2 = 0.41, $P < .0001$; STOC: R^2 = 0.48, $P < .0001$; LC: R^2 = 0.62, $P < .0001$). The relationship was cleanest for the LC scheme with a monotonic and near-linear relationship observed between LC stage and global SUVr (Fig. 5).

3.4. Relationship to disease stage and amyloid status

The distribution of assigned tau PET stages across disease stage and amyloid status is illustrated for each staging

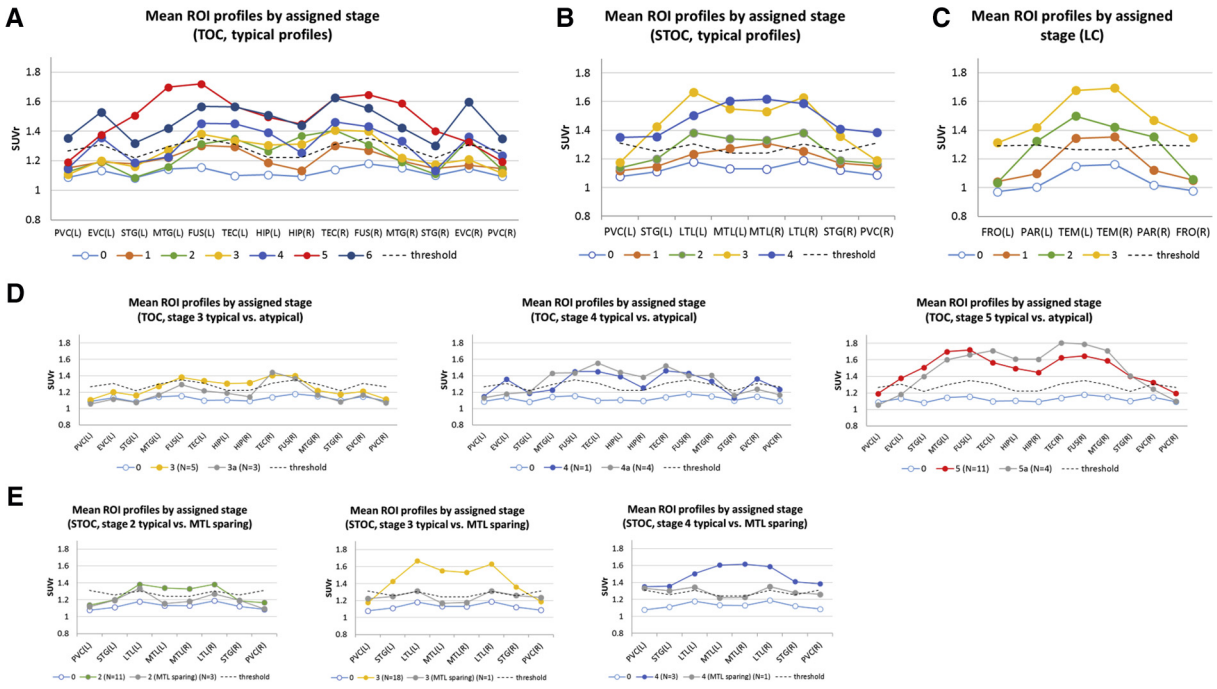

Fig. 2. Mean ROI profiles for each assigned stage across the three staging schemes in the ADNI-2 data set. (A–C) Typical patterns for the (A) TOC, (B) STOC, and (C) LC schemes. (D, E) Atypical vs. typical profiles observed for (D) TOC and (E) STOC schemes. Abbreviations: ROI, region of interest; ADNI, Alzheimer's Disease Neuroimaging Initiative; TOC, Temporal-Occipital Classification; STOC, Simplified Temporal-Occipital Classification; LC, lobar classification; PVC, primary visual cortex; EVC, extrastriate visual cortex; STG, superior temporal gyrus; MTG, middle temporal gyrus; FUS, fusiform gyrus; TEC, transentorhinal cortex; HIP, hippocampus; MTL, mesial temporal lobe; LTL, lateral temporal lobe; TEM, temporal lobe; PAR, parietal lobe; FRO, frontal lobe; SUVr, standardized uptake value ratio.

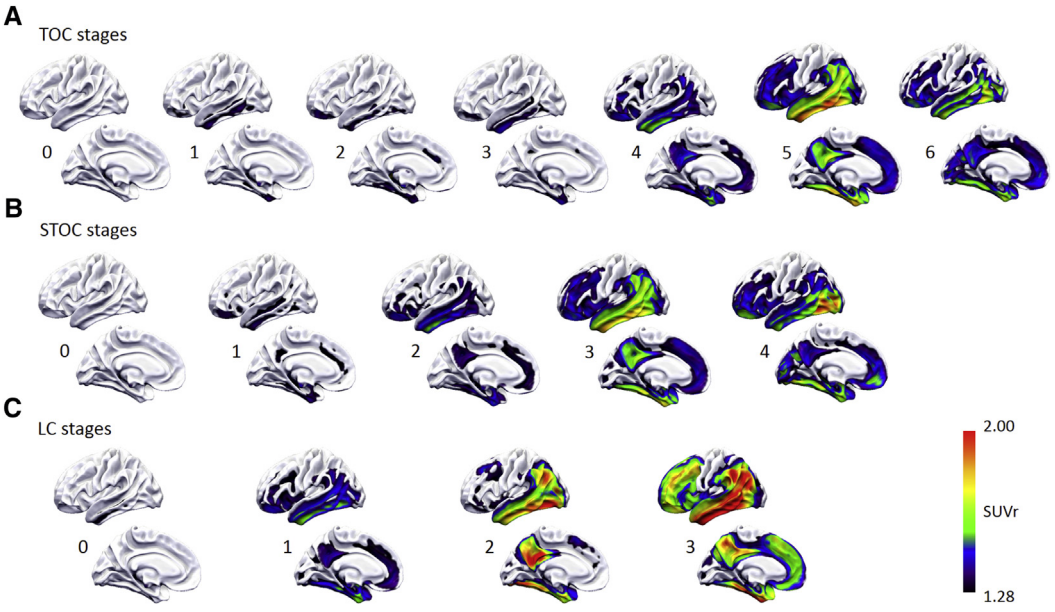

Fig. 3. Mean SUVr maps by assigned stage for the three classification schemes in the ADNI-2 data set. (A) TOC, (B) STOC, and (C) LC shown for left hemisphere. Typical and atypical images for each stage are combined here but are presented separately in the Supplementary Material. Abbreviations: ADNI-2, Alzheimer's Disease Neuroimaging Initiative 2; TOC, Temporal-Occipital Classification; STOC, Simplified Temporal-Occipital Classification; LC, lobar classification; SUVr, standardized uptake value ratio.

scheme in Fig. 6. In all three cases, more advanced tau imaging stages were significantly more prevalent in amyloid positive than amyloid negative participants (TOC, $P = .00029$; STOC, $P = .00013$; LC, $P < .0001$). There was no significant association between disease stage and tau PET stage.

When the classification results were dichotomized to T− or T+, there was a high degree of concordance across the three schemes. Of the 79% (77/98) scans for which the TOC scheme was able to match a profile, 65% (50/77) were classified as T− and 35% (27/77) T+. Both the STOC and LC schemes classified 61/98 (62%) subjects as T− and 37/98 (38%) as T+. There was a 92% concordance between TOC and STOC, 94% between TOC and LC, and 90% between STOC and LC (where the concordance with TOC was calculated only on the 77 scans for which a stage was available for both).

Of the participants whose amyloid status was known, 96%, 82%, and 91% of the subjects classified as T+ by TOC, STOC, and LC, respectively, were also A+; in contrast, 41%, 40%, and 35% of subjects classified as T− by the three methods were A+.

4. Discussion

Image-based topographic tau PET staging schemes can provide a concise summary of how the tau PET signal is distributed across AD-related brain regions and might be a useful complement to other biomarkers and clinical assessments. We evaluated three different topographic staging schemes on flortaucipir F 18 scans in a test-retest scenario and from subjects from the ADNI-2 tau PET pilot study. The three schemes were largely consistent (90%–94% concordance) when dichotomized to categorize scans as T− or T+. Most (82%–96%) of individuals determined as T+ were also A+, in contrast to only 35% to 41% of individuals determined as T−. Overall, moving toward fewer, larger ROIs and simpler decision rules resulted in more consistent stage assignments across test and retest scans and fewer unclassified or atypical profiles.

The TOC and STOC schemes have most of their dynamic range associated with the earlier phases of AD-related tau accumulation, distinguishing differential involvement of anterior temporal lobe regions before substantial spread to the wider neocortex. The STOC scheme did not attempt to distinguish differential involvement of mesial temporal subregions captured in TOC stages 1–3 because these may be a feature of normal aging [26] and the onset of measurable cognitive symptoms may be associated with the appearance of tau in the lateral temporal regions [9]. Other brain regions commonly observed in association with tau outside the mesial temporal lobe, such as the precuneus and orbitofrontal cortex, and visible in the stage-specific images in Fig. 3, were not explicitly used in these schemes. However, a wide range of neocortical tau patterns are unlikely to be distinguished by the more advanced TOC or STOC stages. Thus, classification schemes like TOC or STOC might be more useful in the study of populations very early in the course of disease (e.g., preclinical AD), where sensitivity to the early spread of tau in the anterior temporal lobe may be of particular interest. However, the present study shows that this sensitivity to more precise regional involvement

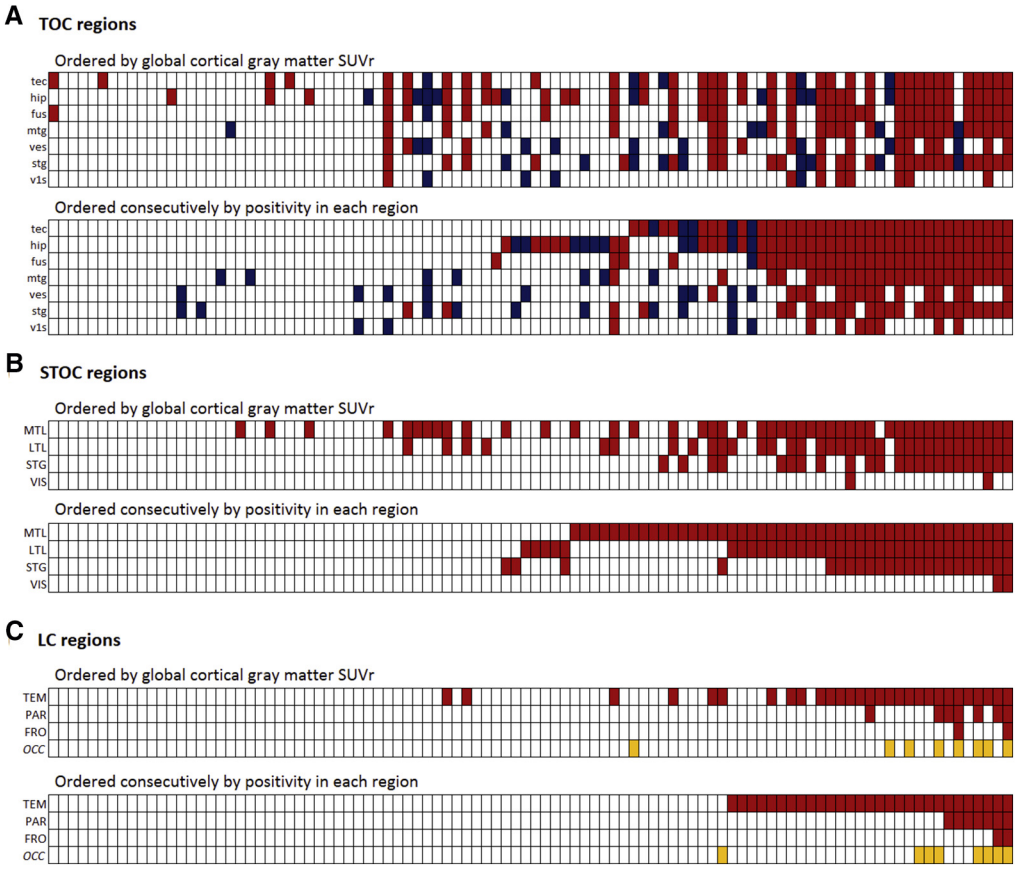

Fig. 4. Stereotypy of regional profiles for the three staging schemes in the ADNI-2 data set. Relationship between regional positivity in the regions used in the TOC (A), STOC (B), and LC (C) regional staging schemes in the ADNI-2 data set. Each column represents an individual scan, with regional positivity reflected by dark shading. In (A), scans that did not match an expected profile are shaded in dark blue. In (C), occipital lobe region positivity is shown in orange as it was not formally used in the LC staging scheme. Regions depicted are bilateral averages; similar patterns were observed when considering each hemisphere independently—see Supplementary Material. Abbreviations: SUVr, standardized uptake value ratio; ADNI-2, Alzheimer's Disease Neuroimaging Initiative 2; TOC, Temporal-Occipital Classification; STOC, Simplified Temporal-Occipital Classification; LC, lobar classification.

may bring with it an increased risk of misclassification due to image noise. In contrast, the LC scheme is likely to be relatively insensitive to differential levels of tau localized to the anterior temporal lobe but, given its more linear relationship with global tau burden and explicit sampling of the wider neocortex, may have more utility in the more advanced stages of tau accumulation. It is also likely that the larger ROIs used in the LC method are relatively

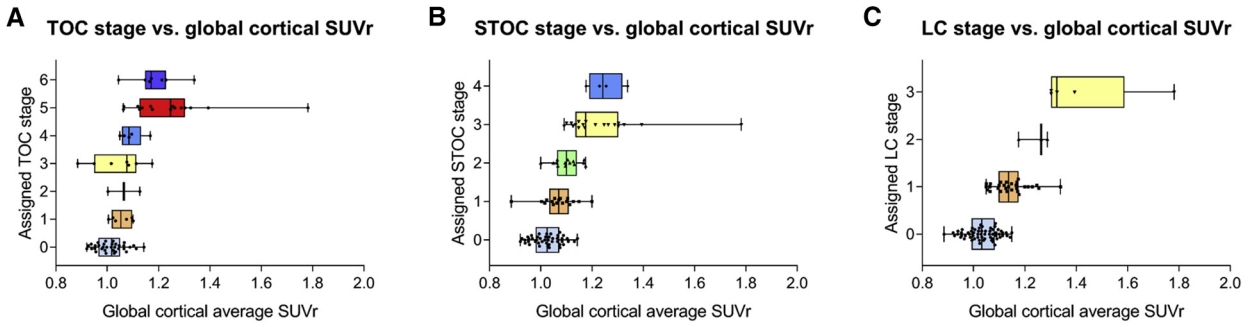

Fig. 5. Relationship between assigned stages and global average SUVr for the three staging schemes in the ADNI-2 data set. (A) TOC stage, (B) STOC stage, and (C) LC stage. In each group, the boxes summarize 25th, 50th, and 75th percentiles, and the whiskers extend from minimum to maximum. Both typical and atypical profiles are included in the TOC (A) and STOC (B) graphs. Abbreviations: SUVr, standardized uptake value ratio; ADNI-2, Alzheimer's Disease Neuroimaging Initiative 2; TOC, Temporal-Occipital Classification; STOC, Simplified Temporal-Occipital Classification; LC, lobar classification.

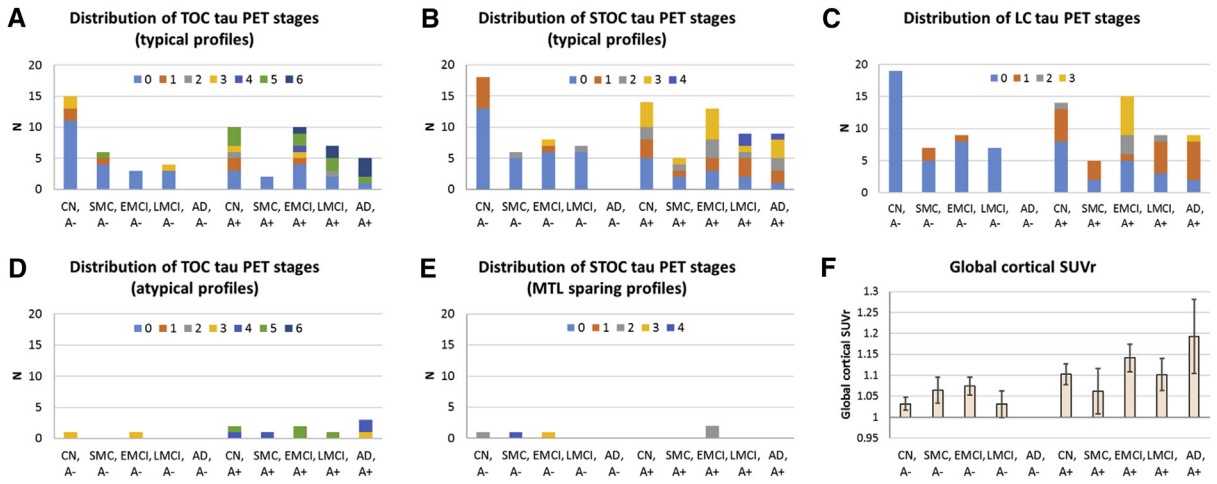

Fig. 6. Distribution of assigned tau PET stages across clinical diagnostic categories and amyloid status in the ADNI-2 data set. (A–C) Typical profiles estimated using (A) TOC, (B) STOC, and (C) LC staging; (D, E) atypical profiles estimated using (D) TOC and (E) STOC. (F) Mean ± standard error of the mean of the global cortical average SUVr, by diagnostic category and amyloid status. Abbreviations: PET, positron emission tomography; SUVr, standardized uptake value ratio; ADNI-2, Alzheimer's Disease Neuroimaging Initiative 2; TOC, Temporal-Occipital Classification; STOC, Simplified Temporal-Occipital Classification; LC, lobar classification; A+, amyloid positive; A−, amyloid negative; CN, cognitively normal; SMC, subjective memory complaint; EMCI, early MCI; LMI, late MCI; AD, Alzheimer's disease.

insensitive to noise-related variations in tau PET signal within subjects and to localized variations in tau pattern between subjects.

In the LC scheme, positivity in the occipital lobe was found in a subset of scans in conjunction with all observed combinations of temporal, parietal, and frontal lobe positivity in the present study. This may be because the whole occipital lobe includes contributions from both lateral and medial parts of the occipital lobe, which can be involved at different stages of tau spread in AD [4]. Occipital lobe tau binding may indicate posterior cortical atrophy [27,28] or might also represent a contribution from concomitant Lewy body pathology, as indicated by a recent tau imaging study in Lewy body dementia [29] and observed occipital hypometabolism noted in individuals with pathologically confirmed Lewy body copathology [30].

The thresholds used for ROI-wise binarization in this study were chosen for consistency with our previous report [10]. The use of lower thresholds would result in more ROIs being positive and would be expected to shift the overall distribution of assigned stages higher. However, it may also lead to increased "false positive" ROIs and potentially to an increased number of profiles that do not fit an expected pattern. The threshold value(s) will also likely depend on the SUVr reference region. In particular, a flortaucipir reference region based on pixels exhibiting behavior suggestive of nonspecific binding in the white matter has recently been proposed for flortaucipir F 18 scans [31]. The question of threshold definition remains open. Clinical correlations and relationship to disease progression can provide information on the thresholds that may be most clinically relevant.

The predominantly stereotypical presentation of tau pathology in AD is the primary rationale behind topographic staging schemes. However, neuropathology studies have also noted some degree of case-to-case variability [1,4,5], and others have proposed specific subtypes of AD based on variant presentations of tau (e.g., hippocampal sparing or limbic predominant) [32]. The TOC and STOC schemes both allowed for limited number of atypical profiles, mainly based on sparing of medial temporal structures or the extrastriate visual cortex. Recent tau PET imaging studies in atypical variants of AD (such as logopenic variant primary progressive aphasia, posterior cortical atrophy, and early-onset AD) have shown anatomical profiles of flortaucipir F 18 binding that differ still more substantially from those observed in amnestic AD [27,33–35]. The LC approach may be best placed to identify these AD variants that appear to have distinct tau PET presentations in the neocortex that can be efficiently summarized on the basis of differential lobar involvement.

Although this PET tracer exhibits robust test-retest performance when assessed using conventional regional methods [24], the three staging schemes assessed here evidenced different sensitivity to scan-to-scan variability in SUVr. The TOC scheme had the worst test-retest consistency in assigned stages, with quite different stage classifications observed for some subjects (e.g., stage 0 to atypical stage 4). It is likely that this reflects both the small size of the ROIs (with potential contributions from both inherent signal variability and slight scan-to-scan differences in image alignment) and the number of ROIs on which the staging is based (higher chance of a variability-induced change between positive and negative in one or more of the regions when the signal intensities are perithreshold). The results with the STOC and LC schemes bear out our hypothesis that a combination of larger regions (reducing the test-

retest variability in image noise per se) and fewer regions (reducing the combinatorial chances of a perithreshold signal changing state) would result in a more robust performance. These findings also highlight the importance of assessing test-retest variability of staging and other analytical methods that depart from conventional ROI analyses.

Limitations of the present study include the limited sample sizes, especially in the more severely symptomatic categories (amnestic MCI and AD). Whereas the results with the TOC scheme were qualitatively consistent with those previously reported in an independent data set [10], further study of these approaches in other data sets is warranted. The staging schemes were designed to assess AD-related tau pathology and assessed here only in well-defined research cohorts targeting older participants in the aged or sporadic AD spectrum; their applicability and performance in more general aging populations, early-onset, or autosomal-dominant patients or in clinical practice remains to be evaluated.

In conclusion, tau PET staging schemes could be useful tools to concisely index the regional involvement of tau pathology in living subjects and as the basis of a dichotomized definition of tau positive or tau negative. Simpler schemes are likely to be more robust. Algorithms such as STOC based on temporal lobe subregions may be more sensitive to early AD-related tau spread, whereas sampling the wider neocortex such as in the LC scheme may be more useful in participants with a greater overall tau burden.

Acknowledgments

Drs. Adam Schwarz, Sergey Shcherbinin, Lawrence Slieker, and Arnaud Charil are full-time employees and minor stockholders of Eli Lilly and Company. Mr. Abhinay Joshi and Drs. Sudeepti Southekal and Michael Devous are full-time employees of Avid Radiopharmaceuticals, a wholly owned subsidiary of Eli Lilly and Company. Dr. Shannon Risacher received support from the following NIH grants: P30 AG010133 and K01 AG049050, as well as the Alzheimer's Association, the Indiana University Health-Indiana University School of Medicine Strategic Research Initiative, and the Indiana Clinical and Translational Science Institute (CTSI). Dr. Andrew Saykin received support from the following NIH grants: U01 AG032984, P30 AG010133, R01 AG019771, R01 LM011360, R44 AG049540, and R01 CA129769. He also received collaborative grant support from Eli Lilly during the conduct of the study. In addition, PET tracer precursor support was provided by Avid Radiopharmaceuticals outside the scope of the submitted work. Dr. Saykin also acknowledges support from Springer Nature as editor-in-chief of Brain Imaging and Behavior. The authors acknowledge an anonymous reviewer for the suggestion to quantify stereotypy using rank correlations.

Supplementary data

Supplementary data related to this article can be found at https://doi.org/10.1016/j.dadm.2018.01.006.

RESEARCH IN CONTEXT

1. Systematic review: The literature on neuropathology and more recent positron emission tomography (PET) imaging reports of the presentation of tau pathology in the human brain and its association with aging and clinical presentations of Alzheimer's disease was reviewed via PubMed search. Specifically, previous work on how Alzheimer's disease tau patterns can be interpreted within a disease staging framework were evaluated.
2. Interpretation: Our work adds to the body of knowledge in this area by assessing methodological robustness (including test-retest reliability) and association with disease stage and amyloid status of three in vivo tau PET staging schemes.
3. Future directions: It will be important to test the generalizability of these findings as more tau PET data accumulate, including with other tau PET radiotracers, and to evaluate the optimal choice of binarization threshold.

References

[1] Braak H, Braak E. Neuropathological stageing of Alzheimer-related changes. Acta Neuropathol 1991;82:239–59.
[2] Thal DR, Rub U, Orantes M, Braak H. Phases of Abeta-deposition in the human brain and its relevance for the development of AD. Neurology 2002;58:1791–800.
[3] Montine TJ, Phelps CH, Beach TG, Bigio EH, Cairns NJ, Dickson DW, et al. National Institute on Aging-Alzheimer's Association guidelines for the neuropathologic assessment of Alzheimer's disease: a practical approach. Acta Neuropathol 2012;123:1–11.
[4] Braak H, Alafuzoff I, Arzberger T, Kretzschmar H, Del Tredici K. Staging of Alzheimer disease-associated neurofibrillary pathology using paraffin sections and immunocytochemistry. Acta Neuropathol 2006;112:389–404.
[5] Delacourte A, David JP, Sergeant N, Buee L, Wattez A, Vermersch P, et al. The biochemical pathway of neurofibrillary degeneration in aging and Alzheimer's disease. Neurology 1999;52:1158–65.

[6] Villemagne VL, Fodero-Tavoletti MT, Masters CL, Rowe CC. Tau imaging: early progress and future directions. Lancet Neurol 2015; 14:114–24.
[7] Saint-Aubert L, Lemoine L, Chiotis K, Leuzy A, Rodriguez-Vieitez E, Nordberg A. Tau PET imaging: present and future directions. Mol Neurodegener 2017;12:19.
[8] Dani M, Brooks DJ, Edison P. Tau imaging in neurodegenerative diseases. Eur J Nucl Med Mol Imaging 2016;43:1139–50.
[9] Johnson KA, Schultz A, Betensky RA, Becker JA, Sepulcre J, Rentz D, et al. Tau PET imaging in aging and early Alzheimer's disease. Ann Neurol 2016;79:110–9.
[10] Schwarz AJ, Yu P, Miller BB, Shcherbinin S, Dickson J, Navitsky M, et al. Regional profiles of the candidate tau PET ligand 18F-AV-1451 recapitulate key features of Braak histopathological stages. Brain 2016;139:1539–50.
[11] Schöll MS, Lockhart N, Schonhaut DR, O'Neil JP, Janabi M, Ossenkoppele R, et al. PET imaging of tau deposition in the aging human brain. Neuron 2016;89:971–82.
[12] Cho H, Choi JY, Hwang MS, Kim YJ, Lee HM, Lee HS, et al. In vivo cortical spreading pattern of tau and amyloid in the Alzheimer's disease spectrum. Ann Neurol 2016;80:247–58.
[13] Pontecorvo MJ, Devous MD Sr, Navitsky M, Lu M, Salloway S, Schaerf FW, et al. Relationships between flortaucipir PET tau binding and amyloid burden, clinical diagnosis, age and cognition. Brain 2017; 140:748–63.
[14] Sperling RA, Aisen PS, Beckett LA, Bennett DA, Craft S, Fagan AM, et al. Toward defining the preclinical stages of Alzheimer's disease: recommendations from the National Institute on Aging-Alzheimer's Association workgroups on diagnostic guidelines for Alzheimer's disease. Alzheimers Dement 2011;7:280–92.
[15] Jack CR, Knopman DS, Jagust WJ, Petersen RC, Weiner MW, Aisen PA, et al. Tracking pathophysiological processes in Alzheimer's disease: an updated hypothetical model of dynamic biomarkers. Lancet Neurol 2013;12:207–16.
[16] Jack CR Jr, Bennett DA, Blennow K, Carrillo MC, Feldman HH, Frisoni GB, et al. A/T/N: An unbiased descriptive classification scheme for Alzheimer disease biomarkers. Neurology 2016; 87:539–47.
[17] Jack CR Jr, Vemuri P, Wiste HJ, Weigand SD, Aisen PS, Trojanowski JQ, et al. Evidence for ordering of Alzheimer disease biomarkers. Arch Neurol 2011;68:1526–35.
[18] Albert MS, DeKosky ST, Dickson D, Dubois B, Feldman HH, Fox NC, et al. The diagnosis of mild cognitive impairment due to Alzheimer's disease: recommendations from the National Institute on Aging-Alzheimer's Association workgroups on diagnostic guidelines for Alzheimer's disease. Alzheimers Dement 2011; 7:270–9.
[19] McKhann GM, Knopman DS, Chertkow H, Hyman BT, Jack CR Jr, Kawas CH, et al. The diagnosis of dementia due to Alzheimer's disease: recommendations from the National Institute on Aging-Alzheimer's Association workgroups on diagnostic guidelines for Alzheimer's disease. Alzheimers Dement 2011;7:263–9.
[20] Dubois B, Feldman HH, Jacova C, Cummings JL, Dekosky ST, Barberger-Gateau P, et al. Revising the definition of Alzheimer's disease: a new lexicon. Lancet Neurol 2010;9:1118–27.
[21] Jack CR Jr, Knopman DS, Weigand SD, Wiste HJ, Vemuri P, Lowe V, et al. An operational approach to National Institute on Aging-Alzheimer's Association criteria for preclinical Alzheimer disease. Ann Neurol 2012;71:765–75.
[22] Maass A, Landau S, Baker SL, Horng A, Lockhart SN, La Joie R, et al. Comparison of multiple tau-PET measures as biomarkers in aging and Alzheimer's disease. NeuroImage 2017;157:448–63.
[23] Qian J, Hyman BT, Betensky RA. Neurofibrillary tangle stage and the rate of progression of Alzheimer symptoms: modeling using an autopsy cohort and application to clinical trial design. JAMA Neurol 2017;74:540–8.
[24] Devous MD, Joshi AD, Navitsky M, Southekal S, Pontecorvo M, Siderowf A, et al. Test-retest reproducibility for the tau PET imaging agent Flortaucipir F 18 [published online ahead of print December 28, 2017]. J Nucl Med 2017. https://doi.org/10.2967/jnumed.117.200691.
[25] Vemuri P, Lowe VJ, Knopman DS, Senjem ML, Kemp BJ, Schwarz CG, et al. Tau-PET uptake: regional variation in average SUVR and impact of amyloid deposition. Alzheimers Dement (Amst) 2017;6:21–30.
[26] Crary JF, Trojanowski JQ, Schneider JA, Abisambra JF, Abner EL, Alafuzoff I, et al. Primary age-related tauopathy (PART): a common pathology associated with human aging. Acta Neuropathol 2014; 128:755–66.
[27] Ossenkoppele R, Schonhaut DR, Scholl M, Lockhart SN, Ayakta N, Baker SL, et al. Tau PET patterns mirror clinical and neuroanatomical variability in Alzheimer's disease. Brain 2016;139(Pt 5):1551–67.
[28] Day GS, Gordon BA, Jackson K, Christensen JJ, Ponisio MR, Su Y, et al. Tau-PET binding distinguishes patients with early-stage posterior cortical atrophy from amnestic Alzheimer disease dementia. Alzheimer Dis Assoc Disord 2017;31:87–93.
[29] Kantarci KV, Lowe J, Boeve BF, Senjem ML, Tosakulwong N, Lesnick TG, et al. AV-1451 tau and beta-Amyloid PET imaging in dementia with lewy bodies. Ann Neurol 2017;81:58–67.
[30] Toledo JB, Cairns NJ, Da X, Chen K, Carter D, Fleisher A, et al. Clinical and multimodal biomarker correlates of ADNI neuropathological findings. Acta Neuropathol Commun 2013;1:65.
[31] Southekal S, Devous MD, Kennedy I. Flortaucipir F 18 quantitation using a Parametric Estimate of Reference Signal Intensity (PERSI) [published online ahead of print November 30, 2017]. J Nucl Med 2017. https://doi.org/10.2967/jnumed.117.200006.
[32] Murray ME, Graff-Radford N, Ross OA, Petersen RC, Duara R, Dickson D. Neuropathologically defined subtypes of Alzheimer's disease with distinct clinical characteristics: a retrospective study. Lancet Neurol 2011;10:785–96.
[33] Ossenkoppele R, Cohn-Sheehy BI, La Joie R, Vogel JW, Moller C, Lehmann M, et al. Atrophy patterns in early clinical stages across distinct phenotypes of Alzheimer's disease. Hum Brain Mapp 2015; 36:4421–37.
[34] Verfaillie SC, Adriaanse SM, Binnewijzend MA, Benedictus MR, Ossenkoppele R, Wattjes MP, et al. Cerebral perfusion and glucose metabolism in Alzheimer's disease and frontotemporal dementia: two sides of the same coin? Eur Radiol 2015;25:3050–9.
[35] Scholl M, Ossenkoppele R, Strandberg O, Palmqvist S, Jogi J, Ohlsson T, et al. Distinct 18F-AV-1451 tau PET retention patterns in early- and late-onset Alzheimer's disease. Brain 2017;140:2286–94.